Generation of nonclassical light by dissipative two-photon processes

L. Gilles, B. M. Garraway, and P. L. Knight
Optics Section, Blackett Laboratory, Imperial College, London SW7 2BZ, United Kingdom
(Received 20 July 1993)

Nonclassical states of light may be generated by processes involving the creation or annihilation of photons in pairs. A quadratic coupling, characteristic of a parametric amplifier, generates a squeezed vacuum from a normal vacuum, and a two-photon absorber can also generate a squeezed state (though not a minimum-uncertainty state) even though it is a purely dissipative process. We consider here the simultaneous action of a quadratic pump on a two-photon absorber and demonstrate how superpositions of distinct coherent states may be generated by their combined effects. We use standard master equations to describe the time development, employing split operators and direct numerical integrations to determine the field density-matrix elements and quasiprobabilities. The purities of the nonclassical states are determined by evaluating the field entropy. Provided one-photon dissipative processes may be ignored, a pure superposition state is formed in the steady state. This superposition is destroyed if one-photon loss processes are important.

PACS number(s): 42.50.Lc, 42.50.Dv, 32.80.Wr, 42.65.Ky

I. INTRODUCTION

It is well known that dissipation has a very destructive effect on coherence and nonclassical properties of light. Nevertheless, it has recently been found that both coherence *and* nonclassical properties survive when the dissipative process is that of a two-photon absorber [1]. In this paper we study the remarkable properties of a two-photon absorber which is pumped by a two-photon parametric process. In this case we find that if the field starts in the vacuum it evolves into a statistical mixture of states before returning to a pure state (which is not the vacuum). Thus a dissipative process in competition with parametric amplification can produce a pure state with finite energy. These pure states are Schrödinger "cat" states; they are a quantum-mechanical superposition of two coherent states which are out of phase. This feature has been recently studied in Ref. [2] and we discuss this further below.

The two-photon absorber is a very special case and in practice we cannot expect to completely remove the effects of one-photon losses from the field. These effects can be very destructive because they easily destroy coherence, squeezing, and other nonclassical effects. The Schrödinger cat states that are formed by the two-photon absorber with pumping have either even or odd numbered Fock states; the unfortunate effect of the one-photon losses is to spread the photon-number distribution over Fock states of both parities and remove the coherence. We will illustrate this by presenting results for the entropy of the field and its Wigner function. For practical systems we might reduce one-photon losses by using microcavities or photonic band gaps to exclude unwanted modes [3].

In the next section we present the model system within the density-matrix formalism and in Secs. III and IV we show how to solve the problem numerically. Details of the steady-state solution to the master equation are given in Sec. V. Section VI introduces the Wigner quasiprobability function and gives steady-state examples. In Sec. VII we examine the behavior of the Wigner function as a function of time and we also present results on the entropy of the field. In Secs. VIII and IX we give time-dependent results for initial Fock states such as the vacuum. Then in Sec. X we examine the time development for an initial cat state and for an initial thermal field. Section XI concludes this paper.

II. THE MODEL SYSTEM

We analyze the statistical properties of light fields in parametric amplification subjected to incoherent two-photon and one-photon losses. This process is described by the following Liouville equation for a density matrix $\hat{\rho}$:

$$\frac{\partial\hat{\rho}}{\partial t}=\mathcal{L}\hat{\rho}=\mathcal{L}_\lambda\hat{\rho}+\mathcal{L}_1\hat{\rho}+\mathcal{L}_2\hat{\rho}\ , \tag{1}$$

where we have defined the superoperators

$$\begin{aligned}\mathcal{L}_\lambda\hat{\rho}&=-i[\hat{H}_\lambda,\hat{\rho}]\ ,\\ \mathcal{L}_1\hat{\rho}&=-\kappa_1(\hat{a}^\dagger\hat{a}\hat{\rho}+\hat{\rho}\hat{a}^\dagger\hat{a}-2\hat{a}\hat{\rho}\hat{a}^\dagger)\ ,\\ \mathcal{L}_2\hat{\rho}&=-\kappa_2(\hat{a}^{\dagger 2}\hat{a}^2\hat{\rho}+\hat{\rho}\hat{a}^{\dagger 2}\hat{a}^2-2\hat{a}^2\hat{\rho}\hat{a}^{\dagger 2})\ .\end{aligned} \tag{2}$$

The two superoperators $\mathcal{L}_1\hat{\rho}$ and $\mathcal{L}_2\hat{\rho}$ describe the one-photon and two-photon losses with the rates κ_1 and κ_2, respectively. They can be derived from standard master equation theory [4]. The superoperator $\mathcal{L}_\lambda\hat{\rho}$ does not describe losses; it contains the Hamiltonian part of the system which in our case is the coherent parametric pumping. The parametric Hamiltonian is given by

$$\hat{H}_\lambda=\frac{i}{2}(\lambda a^2-\lambda^*\hat{a}^{\dagger 2})\ ,\quad \lambda=|\lambda|e^{i\varphi}\ . \tag{3}$$

For later convenience we define the scaled coupling

$$\Omega=\lambda/\kappa_2 \tag{4}$$

and the scaled time

$$\tau = 2\kappa_2 t \ . \tag{5}$$

We include one-photon losses because in practical situations it may be very difficult to eliminate them. Furthermore, their presence, even if weak, can have a very damaging effect on the production of interesting quantum states through what would otherwise be purely two-photon processes. If the one-photon loss rate is very low we can approximate the master equation (1) by

$$\frac{\partial \hat{\rho}}{\partial t} = \mathcal{L}_\lambda \hat{\rho} + \mathcal{L}_2 \hat{\rho} \tag{6}$$

over time scales such that one-photon losses are negligible ($t \ll 1/\kappa_1$).

The formal solution of Eq. (1) is given by

$$\hat{\rho}(t) = \exp\{\mathcal{L}(t-t_0)\}\hat{\rho}(t_0) \tag{7}$$

when we start from a time t_0. In practice this general solution is not directly useful; we cannot straightaway find time-dependent observables. However, there are expressions for the density operator in special cases. One such case is two-photon absorption [1], i.e., when $\kappa_1 = 0$ and $\lambda = 0$. Later in this paper we will also give details of the steady-state solution for the density matrix when $\kappa_1 = 0$ and $\lambda \neq 0$ (see also Ref. [2]). But apart from these special cases we must resort to numerical methods. We will next describe the two methods we have used: the split operator method and direct solution of the master equation.

III. THE SPLIT-OPERATOR METHOD

In order to take two-photon absorption into account with parametric amplification (neglecting one-photon losses) we have to evaluate the action on the density matrix of the exponential operator in Eq. (7) to describe the combined effects of both processes. Due to the noncommuting nature of the two superoperators $\mathcal{L}_\lambda$ and $\mathcal{L}_2$, the analysis is considerably complicated. We propose therefore an approximate solution by assuming that the two nonlinear effects can act independently over short time steps. Thus given that Eq. (7) may be written as

$$\hat{\rho}(t+\delta t) = \exp\{\mathcal{L}\delta t\}\hat{\rho}(t) \ , \tag{8}$$

we obtain the advancement of the solution over a short time step δt when we approximate this by

$$\hat{\rho}(t+\delta t) \approx \exp\{\mathcal{L}_2 \delta t\}\exp\{\mathcal{L}_\lambda \delta t\}\hat{\rho}(t) \ , \tag{9}$$

if we neglect the one-photon losses. Each time step now takes place in two stages: in the first part, parametric amplification acts alone, in the second part, two-photon absorption acts alone. This procedure is known as the split operator method within the context of numerical solutions of the Schrödinger equation [5] (although our choice of the type of splitting differs from the standard choice in [5] not least because we split superoperators rather than operators).

The technique is equivalent to disentangling the exponential operator (8) into a product of two exponential operators. To estimate the error, we use the Baker-Campbell-Hausdorff formula [6]:

$$\exp\{\hat{A}\}\exp\{\hat{B}\} = \exp\{\hat{A} + \hat{B} + \tfrac{1}{2}[\hat{A},\hat{B}] + \tfrac{1}{12}[\hat{A}-\hat{B},[\hat{A},\hat{B}]] \cdots\} \ . \tag{10}$$

Comparing Eqs. (10) and (9) we see that the dominant error term is quadratic in the step size δt. We can reduce the error to third order in δt if the absorption acts in the middle of two half-steps of amplification rather than separately at the end. Equation (9) is then replaced by

$$\hat{\rho}(t+\delta t) \approx \exp\{\mathcal{L}_\lambda \delta t/2\}\exp\{\mathcal{L}_2 \delta t\}\exp\{\mathcal{L}_\lambda \delta t/2\}\hat{\rho}(t) \ . \tag{11}$$

(The same order of error would be produced by placing the parametric amplification step in the center.) To describe the intermediate steps in Eq. (11) we define

$$\begin{aligned} \hat{\rho}^{(\lambda)}(t) &= \exp\{\mathcal{L}_\lambda \delta t/2\}\hat{\rho}(t) \ , \\ \hat{\rho}^{(\kappa_2)}(t) &= \exp\{\mathcal{L}_2 \delta t\}\hat{\rho}^{(\lambda)}(t) \ . \end{aligned} \tag{12}$$

In order to evaluate each step in Eq. (11) we will decompose the density operator into the Fock basis:

$$\hat{\rho}(t) = \sum_{n,m} \rho_{n,m}(t)|n\rangle\langle m| \ . \tag{13}$$

We start by considering first the parametric amplification step. The action of the driving field can be written in terms of a unitary squeezing operator $\hat{S}(r)$ such that

$$\hat{\rho}^{(\lambda)} = \hat{S}(r)\hat{\rho}\hat{S}^\dagger(r) \ , \tag{14}$$

where $\hat{S}(r)$ is defined from the parametric Hamiltonian $\hat{H}_\lambda$ as

$$\begin{aligned} \hat{S}(r) &= \exp\{-i\hat{H}_\lambda \delta t/2\} = \exp\{\tfrac{1}{2}(r\hat{a}^2 - r^*\hat{a}^{\dagger 2})\} \ , \\ r &\equiv |r|e^{i\varphi} = \lambda \delta t/2 \end{aligned} \tag{15}$$

for a half-step. Inserting into Eq. (14) the expression Eq. (13) of the density operator $\hat{\rho}$ in the Fock basis, we obtain the matrix elements of $\hat{\rho}^{(\lambda)}$:

$$\rho_{i,j}^{(\lambda)} = \sum_{n,m} \rho_{n,m}(t)\mathcal{G}_{i,n}(r)\mathcal{G}_{m,j}(-r) \ , \tag{16}$$

$$\mathcal{G}_{k,m}(r) = \langle k|\hat{S}(r)|m\rangle \ . \tag{17}$$

From now on we restrict ourselves to a *real* parametric coupling constant λ, i.e., we choose the driving field phase $\varphi = 0, \pi$ in Eq. (3). Taking into account our phase choice, we easily verify that the squeezing matrix elements satisfy

$$\mathcal{G}_{k,m}(r) = \mathcal{G}_{m,k}(-r) \ . \tag{18}$$

To calculate explicitly these matrix elements, we disentangle the squeezing operator $\hat{S}(r)$ into [7]:

$$\hat{S}(r) = (\cosh r)^{1/2}\exp\{-\tfrac{1}{2}(\tanh r)\hat{a}^{\dagger 2}\} \times (\cosh r)^{-\hat{a}^\dagger \hat{a}}\exp\{\tfrac{1}{2}(\tanh r)\hat{a}^2\} \ . \tag{19}$$

We then obtain

$$\mathcal{G}_{k,m}(r)=\begin{cases}(m!k!)^{1/2}(-\frac{1}{2}\tanh r)^{(k-m)/2}(\cosh r)^{-m-1/2}\sum_{l=\sigma}\frac{(-1)^l(\sinh r/2)^{2l}}{l!(m-2l)![l+(k-m)/2]!} & \text{for } |k-m| \text{ even}\\ 0 \text{ for } |k-m| \text{ odd },\end{cases} \tag{20}$$

where

$$\sigma=\begin{cases}0 & \text{if } k\geq m\\ (m-k)/2 & \text{if } k<m\end{cases} \tag{21}$$

and $[m/2]$ has the usual meaning of $m/2$ for even m and $(m-1)/2$ for odd m.

We now turn to the two-photon absorption step in Eq. (11). This comprises the second exponential superoperator $\exp\{\mathcal{L}_2\delta t\}$ which will act on $\hat{\rho}^{(\lambda)}$. The solution for this has been given by Simaan and Loudon [8] and the effect of two-photon losses on nonclassical states of light such as squeezed states and even and odd coherent states has been investigated by Gilles and Knight [1]. Following Simaan and Loudon [8], we obtain

$$\begin{aligned}\rho_{n,n+\mu}^{(\kappa_2)}(t) &\equiv\langle n|\exp\{\mathcal{L}_2\delta t\}\hat{\rho}^{(\lambda)}(t)|n+\mu\rangle\\ &=\sum_{k=n}^{(k-n=\text{even})}\xi_{k,n}(\mu)e^{-\lambda_k\delta t}\\ &\quad\times\sum_{m=k}^{(m-k=\text{even})}\eta_{m,k}(\mu)\rho_{m,m+\mu}^{(\lambda)}(t)\ .\end{aligned} \tag{22}$$

The explicit expressions for $\xi_{k,m}$ and $\eta_{m,k}$ are given as follows [8]. We define

$$\sigma=\tfrac{1}{2}(\mu-1)\ , \tag{23}$$

$$\lambda_k=k(k+\mu-1)+\tfrac{1}{2}\mu(\mu-1)\ . \tag{24}$$

For $\mu\neq1$, we have

$$\xi_{k,n}(\mu)=\frac{(k+\sigma)(-1)^{k/2-n/2}2^{n-k}\Gamma(\frac{1}{2}k+\frac{1}{2}n+\sigma)}{[n!(n-\mu)!]^{1/2}\Gamma(\frac{1}{2}k-\frac{1}{2}n+1)\pi^{1/2}}\ , \tag{25}$$

$$\eta_{m,k}(\mu)=\frac{[m!(m+\mu)!]^{1/2}\Gamma(\frac{1}{2}m-\frac{1}{2}k+\frac{1}{2})}{(m-k)!\Gamma(\frac{1}{2}m+\frac{1}{2}k+\sigma+1)}\ . \tag{26}$$

The case $\mu=1$ must be treated separately. We obtain

$$\xi_{k,n}(1)=\frac{(-1)^{(1/2)k-(1/2)n}2^{n-1}k\Gamma(\frac{1}{2}k+\frac{1}{2}n)}{n!(n+1)^{1/2}\Gamma(\frac{1}{2}k-\frac{1}{2}n+1)}\ , \tag{27}$$

$$\eta_{k,n}(1)=\frac{m!(m+1)^{1/2}}{2^{m-\delta(k)}(\frac{1}{2}m+\frac{1}{2}k)!(\frac{1}{2}m-\frac{1}{2}k)!}\ , \tag{28}$$

where

$$\delta(k)=\begin{cases}1 & \text{if } k>0\\ 0 & \text{if } k=0.\end{cases} \tag{29}$$

Comparing Eq. (16) to Eq. (22), we see that contrary to the squeezing transformation, two-photon damping effects propagate through the density matrix only along diagonals.

To obtain the full dynamical evolution of our model we then iterate the two steps given in Eqs. (16) and (22) according to Eq. (11).

IV. DIRECT INTEGRATION

The direct method of integration is very general and can readily include the effect of one-photon losses, but it is restricted to smaller-sized problems than the split operator method. New stochastic wave-function simulation methods [9] may prove to be numerically economical for this problem and their use in this context will be examined elsewhere. We do not evaluate a general solution such as Eq. (7) but instead return to the master equation (1). We express this in a truncated Fock basis to make the problem tractable. In this basis we let $\langle m|\hat{\rho}|n\rangle\equiv\rho_{m,n}$ and find

$$\begin{aligned}\frac{\partial\rho_{m,n}}{\partial t}=&\tfrac{1}{2}[\lambda\sqrt{(m+1)(m+2)}\rho_{m+2,n}-\lambda^*\sqrt{m(m-1)}\rho_{m-2,n}-\lambda\sqrt{n(n-1)}\rho_{m,n-2}+\lambda^*\sqrt{(n+1)(n+2)}\rho_{m,n+2}]\\ &-\kappa_1\{(m+n)\rho_{m,n}-2\sqrt{(m+1)(n+1)}\rho_{m+1,n+1}\}\\ &-\kappa_2\{[m(m-1)+n(n-1)]\rho_{m,n}-2\sqrt{(m+1)(m+2)(n+1)(n+2)}\rho_{m+2,n+2}\}\ .\end{aligned} \tag{30}$$

Thus we have a set of coupled differential equations which can be solved numerically by, for example, the Runge-Kutta method. In what follows we have used this numerical method to determine the influence of the one-photon processes on the system evolution.

V. STEADY-STATE SOLUTION

In the absence of one-photon losses it is possible to find a steady-state solution [2] to the master equation (6) so that $\mathcal{L}\hat{\rho}=0$. We expand the density matrix in the coherent state basis as

$$\hat{\rho}(t=\infty)=\sum_{\alpha,\alpha'}C_{\alpha,\alpha'}|\alpha\rangle\langle\alpha'|\ , \tag{31}$$

where $|\alpha\rangle$ and $|\alpha'\rangle$ are coherent states and $C_{\alpha,\alpha'}$ are constants such that $\hat{\rho}(\infty)$ satisfies the conditions to be a density matrix ($\mathrm{Tr}\hat{\rho}=1$, $\hat{\rho}=\hat{\rho}^\dagger$, and diagonal elements of $\hat{\rho}$ are positive in any basis). If we substitute this trial solution into $\mathcal{L}\hat{\rho}=0$ we find

$$\sum_{\alpha,\alpha'} C_{\alpha,\alpha'}\{(-\lambda/2-[(\alpha')^*]^2\kappa_2)|\alpha\rangle\langle\alpha'|\hat{a}^2 + (-\lambda/2-\alpha^2\kappa_2)\hat{a}^{\dagger 2}|\alpha\rangle\langle\alpha'| + \{\lambda\alpha^2/2+\lambda^*[(\alpha')^*]^2/2 + 2\kappa_2\alpha^2[(\alpha')^*]^2\}|\alpha\rangle\langle\alpha'|\}=0 . \quad (32)$$

This equation is satisfied for each $C_{\alpha,\alpha'}$ if

$$\alpha^2=[(\alpha')^*]^2=\frac{-\lambda}{2\kappa_2}=-\Omega/2 , \quad (33)$$

where we have defined Ω as the scaled coupling λ/κ_2. In what follows we let

$$\beta=\sqrt{-\Omega/2} \quad (34)$$

so that α and α' are each restricted to two values only,

$$\alpha=\pm\beta , \quad \alpha'=\pm\beta , \quad (35)$$

resulting in four possible coefficients $C_{\alpha,\alpha'}$. The steady-state density operator may thus be written as

$$\hat{\rho}(\infty)=C_{\beta,\beta}|\beta\rangle\langle\beta|+C_{\beta,-\beta}|\beta\rangle\langle-\beta| + C^*_{\beta,-\beta}|-\beta\rangle\langle\beta|+C_{-\beta,-\beta}|-\beta\rangle\langle-\beta| . \quad (36)$$

We observe that this density operator is an eigenstate of $\hat{a}^2$.

For now we are neglecting the one-photon operator $\mathcal{L}_1$ and the master equation contains only $\mathcal{L}_\lambda$ and $\mathcal{L}_2$ which both contain the operators $\hat{a}^2$ and $\hat{a}^{\dagger 2}$ rather than $\hat{a}$ and $\hat{a}^\dagger$. As a result, if we work in the Fock basis, we find that even Fock states are only coupled to even Fock states and odd only to odd. Thus it makes sense to separate out the even and odd Fock states from the steady-state solution. We do this by writing the solution in terms of the even and odd coherent states [13,14]:

$$|\beta\rangle_e=N_{\beta,e}^{1/2}(|\beta\rangle+|-\beta\rangle) , \quad |\beta\rangle_o=N_{\beta,o}^{1/2}(|\beta\rangle-|-\beta\rangle) , \quad (37)$$

which have the normalizations

$$N_{\beta,e}^{-1}=2(1+e^{-2|\beta|^2}) , \quad N_{\beta,o}^{-1}=2(1-e^{-2|\beta|^2}) . \quad (38)$$

Various methods have been proposed to generate these states [15]. Thus the general form for $\hat{\rho}(\infty)$ can be written as

$$\hat{\rho}(\infty)=P_e|\beta\rangle_{e\,e}\langle\beta|+P_o|\beta\rangle_{o\,o}\langle\beta| + a_{eo}|\beta\rangle_{e\,o}\langle\beta|+a_{oe}|\beta\rangle_{o\,e}\langle\beta| , \quad (39)$$

where P_e and P_o are the probabilities of finding an even coherent state or an odd coherent state (with $P_e+P_o=1$), and a_{eo} and a_{oe} are coherences (such that $a_{eo}=a_{oe}^*$). We note that if the system starts with only even Fock states (such as with the vacuum) then P_e is one and all of the other components in (39) are zero. The result is a pure state $|\beta\rangle_{e\,e}\langle\beta|$ in the steady state. Likewise, if the system starts in a state composed of only odd Fock states such as $|1\rangle\langle 1|$, it evolves to the odd coherent state $|\beta\rangle_{o\,o}\langle\beta|$ [2].

If the initial state contains both even and odd Fock states a more complicated result is found in which the coherences a_{eo} and a_{oe} need not be zero in the steady state. Because the master equation preserves the trace of the density matrix and because it only connects even and odd Fock states to themselves it preserves the quantities

$$P_e=\sum_{n\ \mathrm{even}}\rho_{n,n} , \quad P_o=\sum_{n\ \mathrm{odd}}\rho_{n,n} \quad (40)$$

throughout the time evolution. These coefficients are exactly the ones appearing in Eq. (39) and so part of the final state is readily found; it represents a statistical mixture of an even coherent state and an odd coherent state, i.e., a mixture of two cats. In Ref. [2] Gerry and Hach claim that the most general solution of the master equation is a pure state which they write in the form of a superposition of two coherent states. However, this is not so if we consider an initial density matrix which is a statistical mixture of, for example, $|0\rangle\langle 0|$ and $|1\rangle\langle 1|$: the final state is then a statistical mixture of an even coherent state and an odd coherent state. The statement of Gerry and Hach is also untrue if the initial state is a coherent superposition of both even and odd Fock states such as the pure state $2^{-1/2}(|0\rangle+|1\rangle)$; in that case we can also demonstrate that the final state is not a pure state by calculating the entropy.

In the following sections we will examine the evolution to the steady state of the system from a variety of initial states containing even Fock states, odd Fock states, or both.

VI. WIGNER FUNCTIONS AND THE STEADY STATE

A graphic and informative way of displaying the states that are generated is by using one of the quasiprobability distributions; we have chosen here the Wigner function. The Wigner function has a number of advantages when compared to other quasiprobabilities. It is never singular and may contain oscillatory fringes that are indicative of nonclassical behavior.

In the case of the exact solutions for the density matrix, such as the Schrödinger cats (39) above, it is possible to determine the Wigner function analytically. However, when we study the time evolution of the density matrix we have only a numerical result expressed in the Fock basis. The method for finding the Wigner function in this case is outlined below.

The Wigner function is defined as the Fourier transform of the symmetrically ordered characteristic function χ which we may define as a sum over elements χ_{mn}:

$$\chi(\xi)=\sum_{n,n=0}^{\infty}\chi_{mn}(\xi)\rho_{mn} , \quad (41)$$

where

$$\chi_{mn}(\xi)=\langle m|e^{\xi a^\dagger}e^{-\xi^* a}|n\rangle\exp(-|\xi|^2/2) . \quad (42)$$

The matrix elements χ_{mn} can be expressed in terms of Laguerre polynomials L_n^{m-n} [10]

$$\chi_{mn}(\xi)=\sqrt{n!/m!}\exp(-|\xi|^2/2)\xi^{m-n}L_n^{m-n}(|\xi|^2) \quad (43)$$

for $m \geq n$. For $m \leq n$ we have $\chi_{mn} = (-1)^{m-n}\chi^*_{nm}$. From this characteristic function we now calculate the Wigner function by means of a Fourier transform which is conveniently performed in polar coordinates. The Wigner function $W(r,\theta)$ may then be written as [11]

$$W(r,\theta) = \sum_{m,n} \rho_{mn} W_{mn}(r,\theta) , \tag{44}$$

where $W_{mn}(r,\theta)$ are the Fourier transforms of $\chi_{mn}(\xi)$:

$$W_{mn}(r,\theta) = \frac{1}{\pi^2}\int_0^\infty R\, dR \int_0^{2\pi} d\phi\, \chi_{mn}(Re^{i\phi}) \times \exp[2irR\sin(\theta-\phi)] . \tag{45}$$

The integral over ϕ can be found from the integral representation of Bessel functions. Then, e.g., for $m \geq n$

$$W_{mn}(r,\theta) = \frac{2}{\pi}\sqrt{n!/m!}\, e^{i(m-n)\theta} \times \int_0^\infty R\, dR e^{-R^2/2} R^{m-n+1} L_n^{m-n}(R^2) \times J_{m-n}(2rR) , \tag{46}$$

and if we now use a table of integrals [12] we obtain the result

$$W_{mn}(r,\theta) = \frac{2}{\pi}(-1)^n\sqrt{n!/m!}\, e^{i(m-n)\theta}(2r)^{m-n} \times e^{-2r^2} L_n^{m-n}(4r^2) \tag{47}$$

for $m \geq n$. The Wigner function is usually displayed in Cartesian coordinates and so conversion to polar coordinates is necessary when using Eqs. (44) and (47).

We will now use the Wigner function to illustrate the steady-state solutions of Sec. V. First we will neglect one-photon losses. Figure 1 shows the steady-state Wigner function for a driving field $\Omega = 8$ when the steady state is an even coherent state. This could be produced, for example, from an initial vacuum state. The two peaks in the Wigner function represent the two components of the Schrödinger cat. The strong fringes between the peaks show that we have a superposition of the components rather than a statistical mixture (when the fringes would be smaller or absent). There is a central fringe peak directly between the two components; this is a feature of an even coherent state. If we reduce the driving field to $\Omega = 2$, as in Fig. 2, we observe that the components of the steady-state cat move towards each other and the number of fringes decreases. As a result the superposition is less pronounced.

If we include one-photon losses we cannot use the exact solutions of Sec. V and must resort to using the numerical methods to determine the steady-state density matrix. We have found that with only two-photon processes we can produce Schrödinger cat states, but we know that one-photon dissipation is very detrimental to such cats [13]. As an example, consider the even coherent state which contains only even Fock states. The action of the one-photon decay operator $\mathcal{L}_1$ is to fill in the odd Fock states between the even ones and thus destroy the cat. The ensuing destruction of coherence between the components of the cat happens on a fast time scale and results in a statistical mixture of two component states [13,14]. As a result the fringes seen in the Wigner functions of Figs. 1 and 2 are lost. Figure 3 shows such a case; the two-photon pumping $\Omega = 8$ is ex-

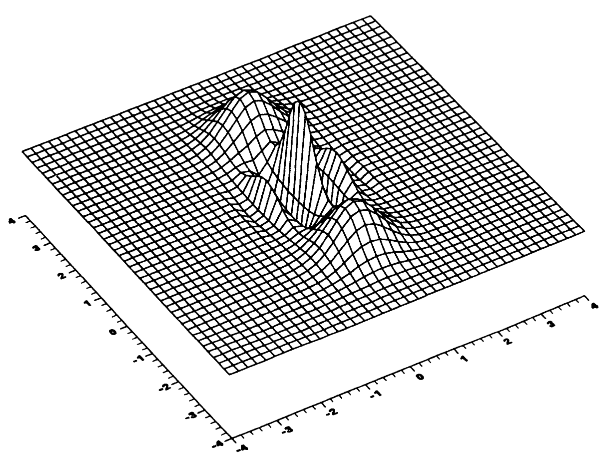

FIG. 1. The steady-state Wigner function for $\Omega=8$ given, e.g, an initial vacuum state. The x axis is on the right and corresponds to $\theta=0$ in Eq. (44).

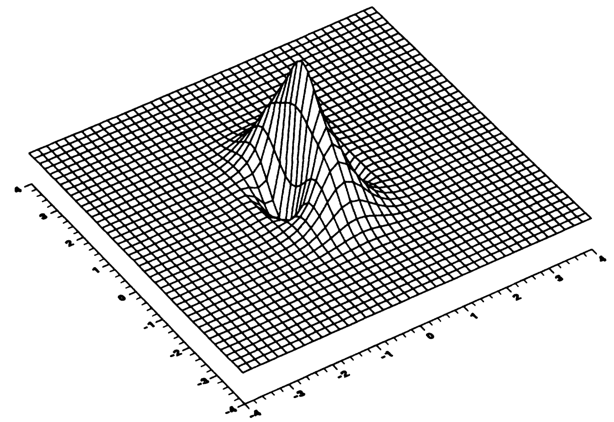

FIG. 2. The steady-state Wigner function for $\Omega=2$ given, e.g., an initial vacuum state.

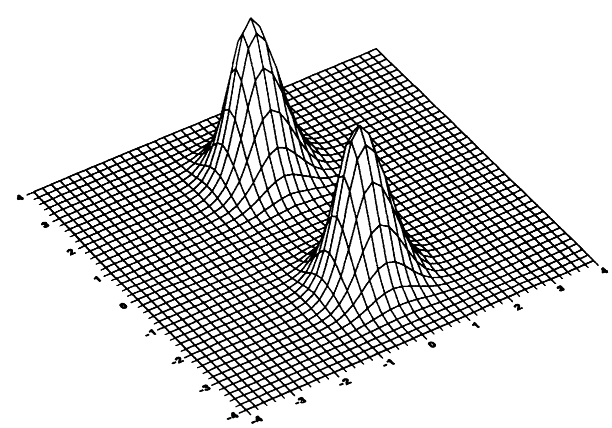

FIG. 3. The steady-state Wigner function in the presence of one- and two-photon losses with $\Omega=8$ and $\kappa_1/\kappa_2=0.125$.

actly the same as in Fig. 1, but in this case there were also one-photon losses at a relative rate of $\kappa_1/\kappa_2=\frac{1}{8}$.

VII. THE FORMATION OF SCHRÖDINGER CATS AND THEIR DECAY

The time development of the Schrödinger cats illustrated in the preceding section follows two distinct stages. The case of $\Omega=8$ without one-photon losses ($\kappa_1=0$) is depicted in Fig. 4. In Fig. 4(a) we see the Wigner function for the initial state. As the initial state is the vacuum, the Wigner function is simply a Gaussian function centered at the origin. During the first moments of the evolution the squeeze operator $\mathcal{L}_\lambda$ plays a significant role. The Wigner function at $\tau=0.5$ is shown in Fig. 4(b) and it shows both squeezing and fringes due to the partial development of two coherent lobes. As time progresses [Figs. 4(c) and 4(d)] the fringes and the lobes separate until we have formed the pure state Schrödinger cat of Fig. 1.

The influence of one-photon dissipation is exhibited in Fig. 5 where we have chosen $\kappa_1/\kappa_2=0.02$ with the same pumping parameter $\Omega=8$ as in Fig. 4. In Fig. 5(a) we already have $\tau=4$, which would be sufficient to reach the steady state if κ_1 were zero. If we compare Fig. 5(a) with Fig. 4(d) we see that in the former case the fringes of the cat are less prominent. As we continue in time [see Figs. 5(b)–5(d)] the fringes steadily die out as the cat is converted into a mixture of (approximately) two coherent states (which we saw in Fig. 3). This has an interesting interpretation in terms of the simulation methods [9] which we will discuss further elsewhere.

A useful way to measure the loss of coherence in the presence of one-photon dissipation is to find the entropy

$$S=-\mathrm{Tr}(\hat{\rho}\ln\hat{\rho}) \ . \tag{48}$$

For a pure state $S=0$ and S increases as coherence is lost. We determine the entropy by a numerical diagonalization of the density matrix. Working in the diagonal basis we can find the logarithm and subsequently the trace and the entropy. Results are shown in Fig. 6. The curve (a) shows the case without one-photon losses (with Wigner functions in Fig. 4). The initial (vacuum) state is a pure state and the entropy rises as the system tries to reach equilibrium. A maximum is reached because when the field reaches the steady state it is in a pure state again (an even coherent state). In (b) we have one-photon losses with $\kappa_1/\kappa_2=0.02$ and we do not expect to reach a pure state as the system evolves (as seen with the Wigner

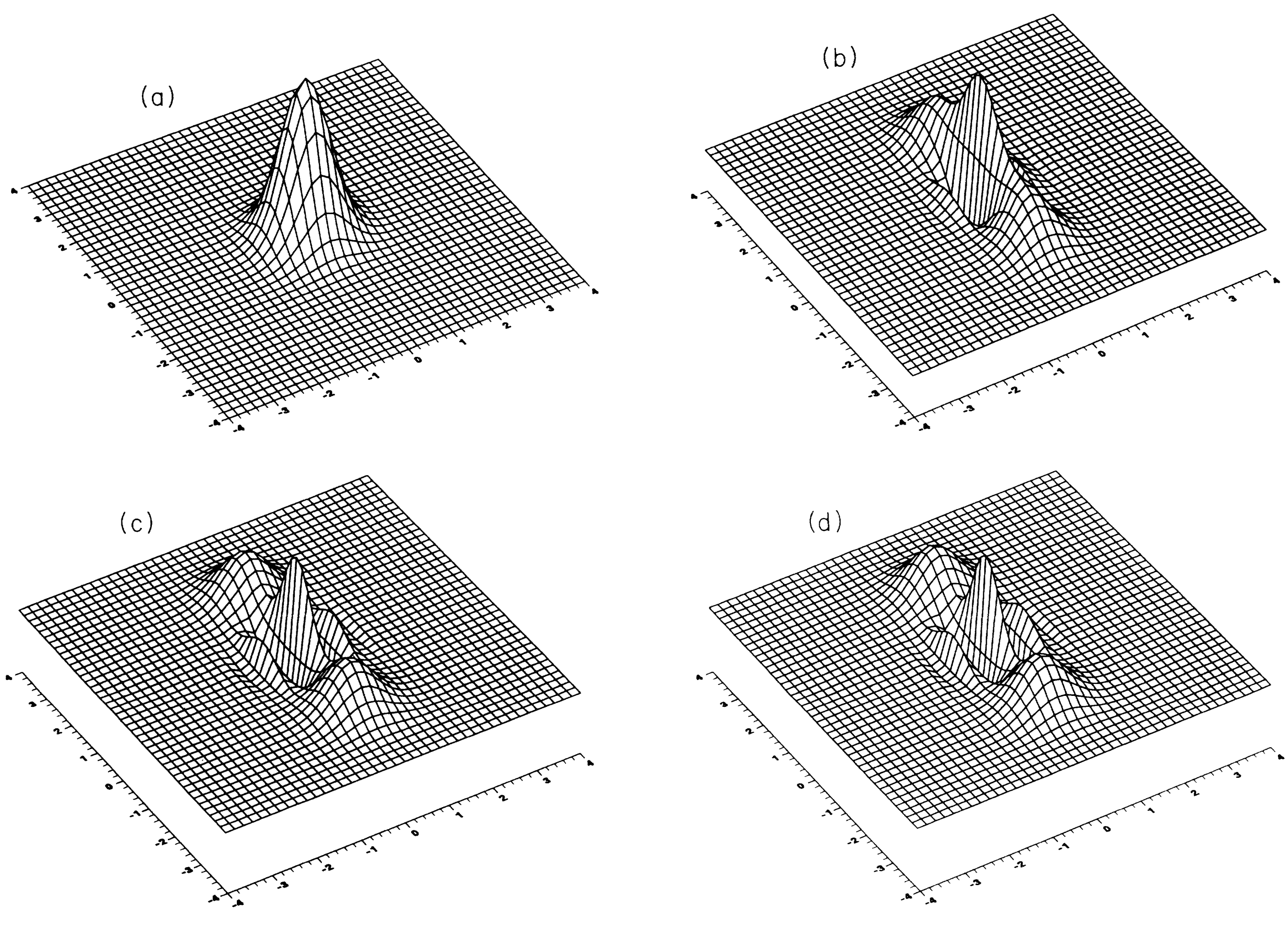

FIG. 4. The time development of the Wigner function for $\Omega=8$ in the absence of one-photon losses ($\kappa_1=0$). The initial state is the vacuum illustrated in (a). The scaled times are (b) $\tau=0.5$, (c) $\tau=1$, and (d) $\tau=1.5$.

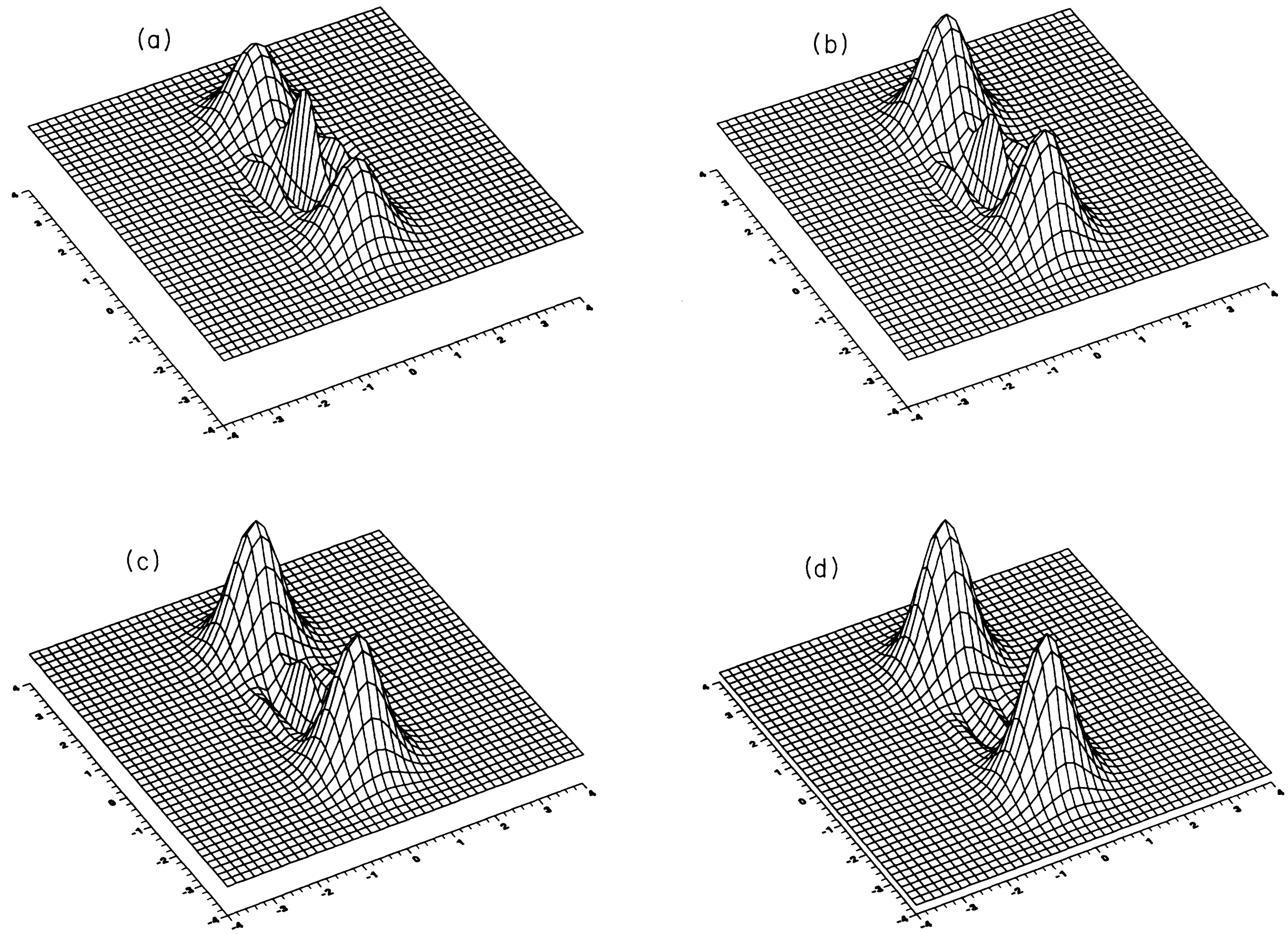

FIG. 5. The late-time development of the Wigner function for $\Omega=8$ in the presence of one-photon losses with $\kappa_1/\kappa_2=0.02$. In (a), (b), (c), and (d) we show $\tau=4$, 8, 12, and 20, respectively.

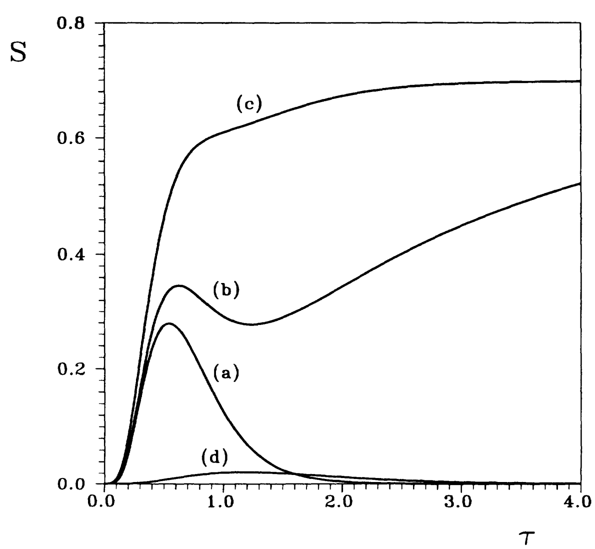

FIG. 6. The entropy of the field for (a) $\Omega=8$ and $\kappa_1=0$, (b) $\Omega=8$ and $\kappa_1/\kappa_2=0.02$, (c) $\Omega=8$ and $\kappa_1/\kappa_2=0.125$, and (d) $\Omega=2$ and $\kappa_1=0$.

functions of Fig. 5). This is confirmed, although the dip in entropy at $\tau\sim 1$ shows that the two-photon processes had some effect in reducing the entropy. However, as time progresses the inevitable destruction of coherence takes place and the entropy rises steadily towards 0.7. This is close to the maximum entropy of a two-level system, $2\ln(2)$, and supports our interpretation that the pure cat state decays into a mixture of two pure states. In (c) the one-photon losses have been increased to $\kappa_1/\kappa_2=0.125$. We see that in this case the entropy rises more rapidly and is not reduced at any stage in the time evolution. The curves (a)–(c) show how sensitive the two-photon production of Schrödinger cats is to one-photon losses. Even in (b) with a one-photon rate which is 50 times smaller than the two-photon loss rate a pure state is never recovered during the time evolution. In both (b) and (c) the increase of entropy in the final stages is very similar to the increase found for field superpositions decaying under the sole influence of one-photon dissipation. However, in the latter case the increase in entropy is eventually followed by a decrease to zero entropy as the state decays to the vacuum without pumping. Finally, the curve (d) in Fig. 6 shows the entropy for a weaker pump with $\Omega=2$ (and $\kappa_1=0$). In this case the entropy does not rise very much, but then the final state is a very weak cat which differs only slightly from the vacuum. A popular measure of the purity of a field is the quantity

$$\xi=1-\mathrm{Tr}(\hat{\rho}^2) , \tag{49}$$

which, like the entropy S, is zero for a pure state and increases for mixed states. It is often calculated instead of the entropy because it is not necessary to diagonalize $\hat{\rho}$. We have found that if we calculate the purity for Fig. 6 the results are quite similar.

VIII. THE NUMBER OPERATOR AND ITS FLUCTUATIONS

The average photon number in the steady state is, for the even and odd coherent state, respectively, given by

$$\langle \hat{n}(\infty)\rangle_e=|\beta^2|\tanh|\beta^2| , \tag{50}$$

$$\langle \hat{n}(\infty)\rangle_o=|\beta^2|/\tanh|\beta^2|>\langle \hat{n}(\infty)\rangle_e , \tag{51}$$

so for $|\beta^2|\gg 1$ the two types of state yield the same mean photon number $\langle \hat{n}\rangle$. We can see this in Fig. 7 where we plot the dynamical evolution of the mean photon number for our choice of scaled couplings Ω. The curve (a) shows the system being driven into an even coherent state after starting in the vacuum. For comparison (aa) shows what happens if the system starts from the Fock state $|1\rangle$ which evolves into an odd coherent state; we eventually obtain about the same final value of $\langle \hat{n}\rangle$. This is not seen if the pump intensity is reduced as in (b) and (bb).

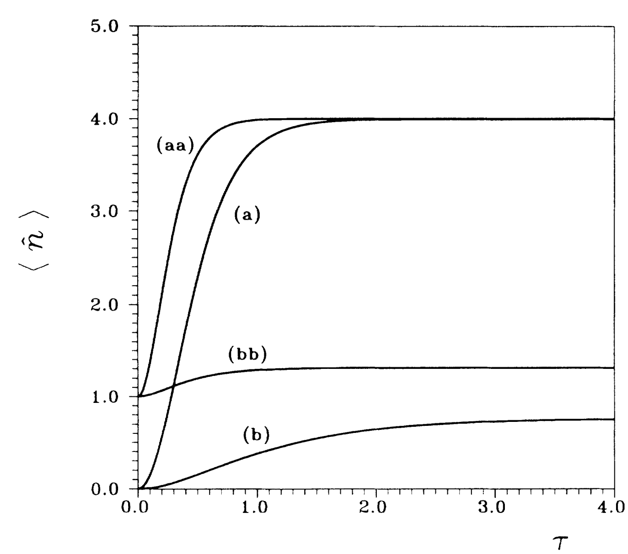

FIG. 7. Mean photon number for initial vacuum and one-photon state labeled by single and double letters, respectively. The scaled coupling is (a) $\Omega=\pm 8$ and (b) $\Omega=\pm 2$, both with $\kappa_1=0$. These curves are invariant under changes of the pump phase φ. At short times the squeezing effect is dominant; then the effect of two-photon absorption takes over until the two processes balance each other. The vacuum evolves towards an even coherent state and the one-photon state evolves towards an odd coherent state. In the limit of large scaled coupling both steady-state mean photon numbers converge to the same value.

The time-dependent results in Fig. 7 are not sensitive to the phase φ of the driving field if the initial state is diagonal in the Fock basis. In part we can see this if we examine the master equation (30). The phase of the pump enters (in λ) if we change diagonals in the density matrix. For example, the transition from the density matrix element $\rho_{m,n}$ to $\rho_{m+2,n}$ or $\rho_{m,n-2}$ under the influence of the Liouville superoperator involves the acquisition of the phase φ in λ. But if there is a following transition to the original diagonal of the density matrix we obtain the factor λ^*, or the phase $-\varphi$, so that the net phase change is zero. This can be shown rigorously in the following way. Consider the transformation

$$\exp(i\hat{n}\varphi/2)\cdots\exp(-i\hat{n}\varphi/2)$$

for which

$$\exp(i\hat{n}\varphi/2)\hat{\rho}\exp(-i\hat{n}\varphi/2)=\hat{\rho}_\varphi \tag{52}$$

and

$$\begin{aligned}\exp(i\hat{n}\varphi/2)\hat{a}\exp(-i\hat{n}\varphi/2)&=\hat{a}e^{-i\varphi/2} ,\\ \exp(i\hat{n}\varphi/2)\hat{a}^\dagger\exp(-i\hat{n}\varphi/2)&=\hat{a}^\dagger e^{i\varphi/2} .\end{aligned} \tag{53}$$

Then it is clear that by using this transformation we can remove the pump phase from the master equation. Thus if the initial density matrix is unaffected by the transformation, changing the pump phase can only affect the time-dependent density matrix by the transformation (52). Then the effect on the mean photon number is given by

$$\mathrm{Tr}(\hat{n}\hat{\rho}_\varphi)=\mathrm{Tr}[\hat{n}\exp(i\hat{n}\varphi/2)\hat{\rho}\exp(-i\hat{n}\varphi/2)]=\langle\hat{n}\rangle , \tag{54}$$

showing that $\langle \hat{n}\rangle$ is independent of the pump phase for a diagonal initial density matrix, i.e., when $\hat{\rho}(0)=\hat{\rho}_\varphi(0)$. However, we note that the average value of observables which are not diagonal in the Fock basis will be sensitive to pump phase changes.

The even coherent state displays photon bunching,

$$\frac{\langle[\Delta\hat{n}(\infty)]^2\rangle_e}{\langle\hat{n}(\infty)\rangle_e}=1+\frac{|\beta^2|}{\sinh|\beta^2|\cosh|\beta^2|}>1 , \tag{55}$$

whereas the odd coherent state displays photon antibunching according to

$$\frac{\langle[\Delta\hat{n}(\infty)]^2\rangle_o}{\langle\hat{n}(\infty)\rangle_o}=2-\frac{\langle[\Delta\hat{n}(\infty)]^2\rangle_e}{\langle\hat{n}(\infty)\rangle_e}<1 . \tag{56}$$

In Fig. 8 we plot

$$\sigma=\frac{\langle[\Delta\hat{n}(t)]^2\rangle}{\langle\hat{n}(t)\rangle} , \tag{57}$$

which shows how photon bunching and antibunching evolve during the interaction. For the initial vacuum state [curves (a) and (b)] σ has a value of 2 close to $\tau=0$, while for the initial Fock state $|1\rangle$ the value of σ at $\tau=0$ is zero [curves (aa) and (bb)]. When the scaled coupling is large enough we obtain a short period of bunching for

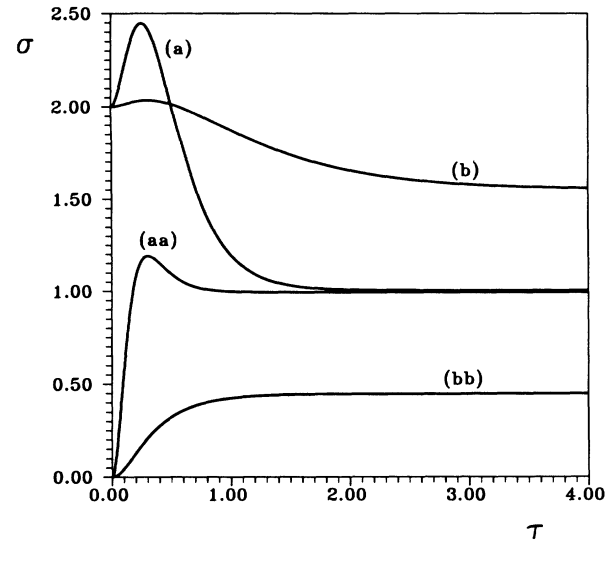

FIG. 8. Relative number variance for the same initial fields, labels, and parameters as in Fig. 7. The steady-state values are given in Eqs. (55) and (56) for the initial vacuum and one-photon state, respectively.

the initial one-photon state, but in the steady state only initial Fock states with an *even* photon number produce bunching [as given in Eq. (55)]. For the same reason as mentioned previously, the relative variance is not sensitive to pump phase changes. At short times, the squeezing effect dominates and leads to enhanced fluctuations in the number operator. On a longer time scale, the effect of two-photon absorption becomes dominant and the relative number variance decreases. In the limit of large Ω the field tends to Poisson photon statistics according to Eqs. (55) and (56).

IX. FIELD QUADRATURES AND SQUEEZING

We are concerned in this section with off-diagonal operators. Due to the two-photon nature of the interaction and given the initial state is diagonal in the Fock basis, the average value of the annihilation and creation operators is zero. However, the steady state (39) is an eigenstate of $\hat{a}^2$ and depending on the sign of β^2 the average value of $\hat{a}^2$ may be positive or negative. Further, the square of the annihilation operator is sensitive to pump phase changes as can be seen from Eq. (53). If φ is changed from 0 to π (i.e., $\Omega \rightarrow -\Omega$) then $\hat{\rho}$ becomes ρ_π [as given in Eq. (52)] and

$$\mathrm{Tr}(\hat{a}^2\hat{\rho}_\pi) = -\langle \hat{a}^2 \rangle \ . \tag{58}$$

We now turn to the field quadratures which are defined by

$$\hat{X}_1 = \frac{(\hat{a}+\hat{a}^\dagger)}{2} \ , \quad \hat{X}_2 = \frac{(\hat{a}-\hat{a}^\dagger)}{2i} \ . \tag{59}$$

In the steady state we have the following fluctuations for the even and odd coherent states:

$$\langle (\Delta\hat{X}_{1,2})^2 \rangle_e = \tfrac{1}{4}\{1 \pm 2|\beta^2|(\beta^2/|\beta^2| \pm \tanh|\beta^2|)\} \ , \tag{60}$$

$$\langle (\Delta\hat{X}_{1,2})^2 \rangle_o = \tfrac{1}{4}\{1 \pm 2|\beta^2|(\beta^2/|\beta^2| \pm 1/\tanh|\beta^2|)\} \ . \tag{61}$$

From these two equations we note that if β^2 is positive then the quadrature $\hat{X}_1$ shows fluctuations above the vacuum level for both types of state. However, $\hat{X}_2$ can display reduced fluctuations, or squeezing, for the even coherent state if β^2 is small, although it will never show squeezing for the odd coherent state [14]. If β^2 is negative, we obtain the same behavior if we interchange $\hat{X}_1$ and $\hat{X}_2$. We need only to analyze one quadrature over our range of coupling constants because our initial states have a diagonal density matrix. We plot in Fig. 9 the uncertainty in $\hat{X}_1$. Although low values of $|\Omega|$ give rise to lower squeezing in the transient regime they give the best squeezing in the steady state for the even coherent state. The initial one-photon state displays reduced fluctuations only in a transient regime on a short time scale if $|\Omega|$ is large. Both states converge to the same limit for large coupling constants because then $\langle \hat{n} \rangle_e \simeq \langle \hat{n} \rangle_o$. We observe in Fig. 10 departure from the minimum-uncertainty product.

X. TIME DEVELOPMENT OF OTHER INITIAL STATES

In this section we analyze the previous statistical properties for two different initial states. We choose an initial even coherent state and an initial thermal field.

Regarding the initial even coherent state, we consider the displacement parameter $\alpha = 2$ so that the state may be denoted as $|2\rangle_e$. Since this state is a superposition of even Fock states, the steady state will be another even

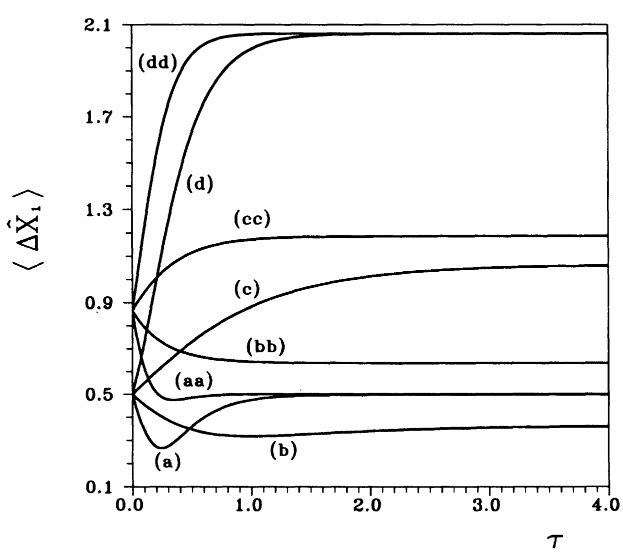

FIG. 9. The uncertainty in the field quadrature $\hat{X}_1$. The single and double letters label the initial vacuum and one-photon state, respectively. We have (a) $\Omega=8$, (b) $\Omega=2$, (c) $\Omega=-2$, and (d) $\Omega=-8$; all are with $\kappa_1=0$. We obtain squeezing in the steady state only over small positive values of Ω. The uncertainty in $\hat{X}_2$ is found by changing the sign of Ω.

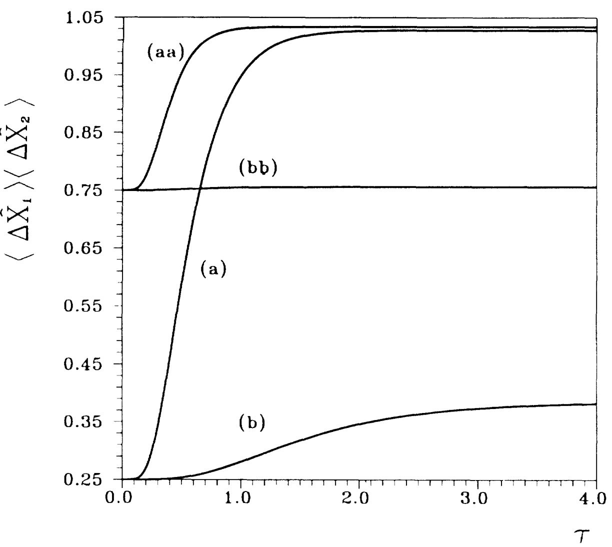

FIG. 10. The product of the uncertainties in the quadratures for the parameters of Fig. 9. In the limit of large coupling $|\Omega|$ the even and odd coherent states display the same uncertainty.

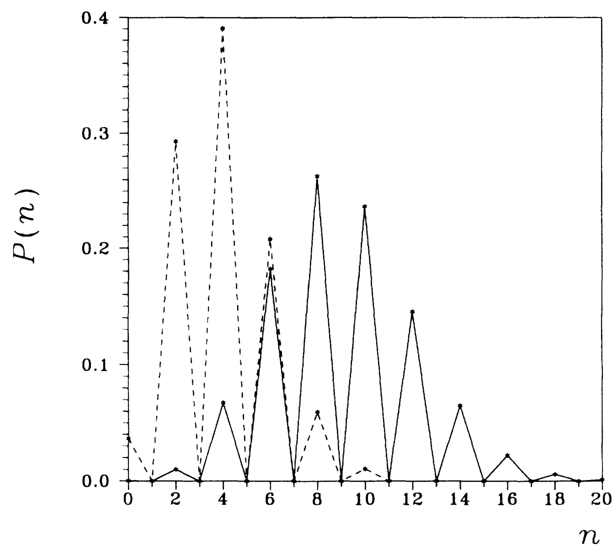

FIG. 11. Photon distributions for an initial even coherent state (dashed lines) with displacement parameter $\alpha=2$ and for the steady state (solid lines) with $|\Omega|=18$. The two-photon nature of the process preserves the oscillations.

coherent state $|\beta\rangle_e$ with β given by Eq. (34). If Ω is positive the two components of the even coherent state are located on the Y axis in phase space according to Eq. (33); if Ω is negative they are located along the X axis. The phase of the pump field determines the position in phase space of the steady state. In what follows we will consider the scaled coupling constants $\Omega=18,2,0,-2,-18$. When $\Omega=0$, we have only two-photon absorption and the result compares with our analysis of nonclassical states of light under two-photon absorption [1].

For the initial thermal field, we choose the initial mean photon number equal to one and the coupling constants $\Omega=\pm 8$ and ± 2. The evolution for the negative coupling values can be found from the positive coupling results by symmetry since the initial field is diagonal in the Fock basis. As a consequence of there being both even and odd Fock states initially, the steady state is a statistical mixture of an even and an odd coherent state. The probabilities P_e, P_o for having, respectively, an even or odd coherent state are given from the conservation rule (40) as

$$P_e=\frac{\bar{n}_{\rm th}+1}{2\bar{n}_{\rm th}+1}\ , \quad P_o=\frac{\bar{n}_{\rm th}}{2\bar{n}_{\rm th}+1}\ , \tag{62}$$

and the coherence $a_{eo}=a_{oe}^*$ is zero. The transfer of population to only two orthogonal states for large time causes the steady-state entropy to be smaller than the initial thermal entropy regardless of the coupling constants. The final entropy is definitely nonzero which as explained in Sec. V contradicts the claim of Gerry and Hach [2] that, in general, the system evolves to a pure state; it only does so for special initial states such as the vacuum.

A. Fluctuations in the number operator

We consider first the intial even coherent state. In Fig. 11 we compare the initial photon distribution (dashed lines) with the steady-state distribution (solid lines) for $|\Omega|=18$. The coherent components of the steady state have a greater amplitude than initially and so the distribution is shifted to the right preserving the oscillations. In Fig. 12 we show the evolution of the mean photon number. Because the initial state is an eigenstate of the two-photon annihilation operator, the density operator is not diagonal in Fock space. Thus we will find that the mean photon number will not be invariant under changes in the pump field phase. This is clearly illustrated for (a) and (e). In (a) the state rotates by $\pi/2$ during its amplification whereas in (e) it remains located along the X axis. When $\Omega=0$ the state relaxes to the vacuum. In Fig. 13 we plot the evolution of the relative variance σ.

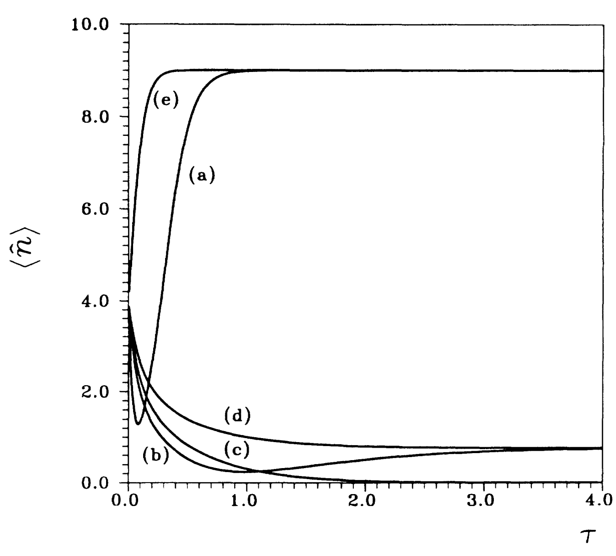

FIG. 12. Mean photon number for an initial even coherent state with displacement $\alpha=2$. The parameters are (a) $\Omega=18$, (b) $\Omega=2$, (c) $\Omega=0$, (d) $\Omega=-2$, and (e) $\Omega=-18$.

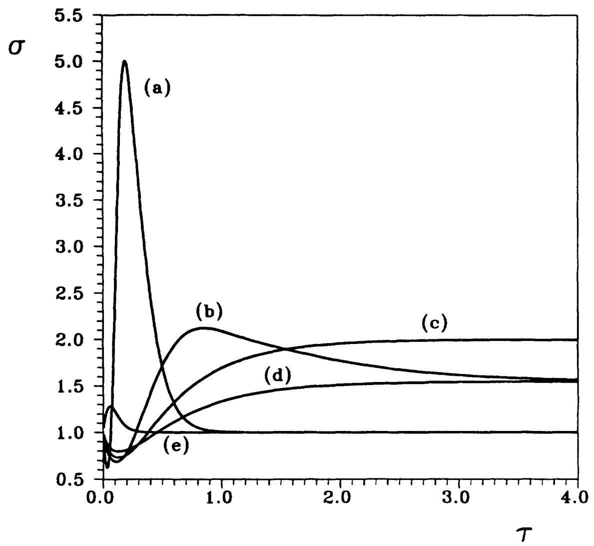

FIG. 13. Relative number variance for the same state and parameters as in Fig. 12. We note the very different behavior of (a) and (d), which differ only by a sign in the coupling constant. The state shows antibunching on a short time scale due to the squeezing effect, except for large negative values of Ω. It is worth mentioning that when (a) reaches its maximum degree of antibunching, the noise in the quadrature $\hat{X}_2$ is squeezed (see Fig. 18) and when it reaches its maximum degree of bunching, the quadrature $\hat{X}_1$ is squeezed see (Fig. 17).

We observe the very different behavior under phase changes of the driving field, especially when comparing (a) and (e). The steady state displays photon bunching according to Eq. (55).

We now turn to the initial thermal field. In Fig. 14 we plot the steady-state photon distribution resulting from

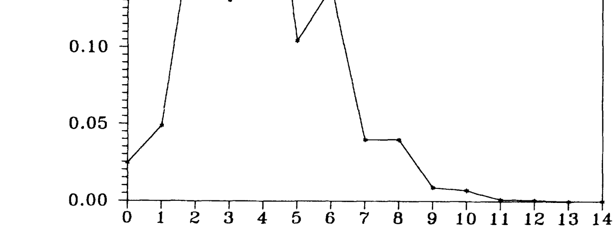

FIG. 14. Steady-state photon statistics for an initial thermal field with $\bar{n}_{th}=1$. The relative coupling is $|\Omega|=8$. The distribution presents oscillations and a maximum. The steady state is a statistical mixture of an even coherent state (with a dominant weight of $\frac{2}{3}$) and an odd coherent state.

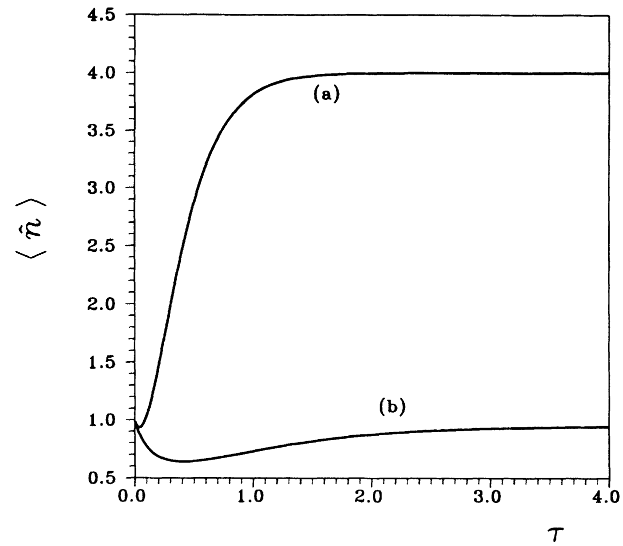

FIG. 15. Mean photon number evolution for an initial thermal field with $\bar{n}_{th}=1$. The parameters are (a) $|\Omega|=8$ and (b) $|\Omega|=2$. The mean energy first decreases, reaches a minimum, and then increases to its steady-state value.

an initial thermal field with $\bar{n}_{th}=1$ and a scaled coupling $\Omega=8$. There are some oscillations even though the steady state consists of a statistical mixture of the two different Schrödinger cat states with interleaving zeros of their photon-number distributions. This is due to the different weightings of the coherent state components of the two cat states and it suggests that some nonclassical behavior exists. The evolution of the mean number of photons is displayed in Fig. 15. The field initially loses energy on a time scale depending on the coupling parameter. The stronger is the coupling, the shorter is the decrease in the mean number. After reaching a minimum value, the mean number increases towards its steady-state value given by

$$\langle \hat{n}(\infty)\rangle = P_e\langle \hat{n}(\infty)\rangle_e + P_o\langle \hat{n}(\infty)\rangle_o \ , \qquad (63)$$

where $\langle \hat{n}(\infty)\rangle_e$ and $\langle \hat{n}(\infty)\rangle_o$ are given in Eqs. (50) and (51), respectively, and P_e and P_o are given in Eq. (62). Figure 16 shows the evolution of the relative variance in the number operator. We observe the very different behavior at short times. When $|\Omega|$ is large enough, the relative variance presents a nonmonotonic behavior in contrast with the monotonic decrease in the case of small $|\Omega|$. For $|\Omega|\gg 1$, the steady-state photon statistics is Poissonian.

B. Fluctuations in off-diagonal operators

Again, we first consider the intial even coherent state. Figures 17 and 18 show how the noise in the field quadratures $\hat{X}_1$ and $\hat{X}_2$, respectively, evolves. Only when $\Omega=0$ do we reach the vacuum level. The fluctuations in $\hat{X}_1$ are reduced except for large negative values of Ω. Only (a) is a nonmonotonic curve in Fig. 17. In Fig. 19 we plot the product of the standard deviation in $\hat{X}_1$ and $\hat{X}_2$. When Ω is positive the curves display a minimum. Finally we

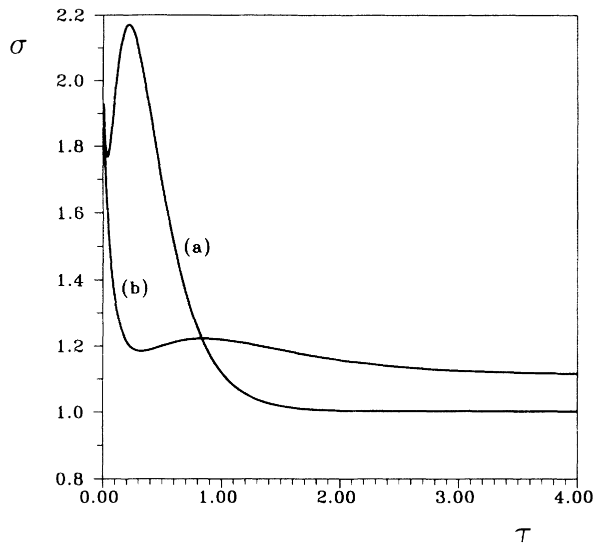

FIG. 16. Number variance relative to the mean number for the same initial conditions as in Fig. 15. We note the very different behavior at short times, depending on the coupling strength. In the limit of large $|\Omega|$, the field tends to a Poisson photon statistics.

show in Fig. 20 the evolution of the field purity defined in Eq. (49). We note that when Ω is positive, i.e., when the state rotates during its evolution, the deviation from a pure state is maximal.

For the initial thermal field the evolution of the fluctuations in the field amplitude $\hat{X}_1$ is presented in Fig. 21 for the same parameters as in Fig. 15. By symmetry, if we change the sign of Ω, we obtain the fluctuations in the other quadrature $\hat{X}_2$. The initial value is obtained from

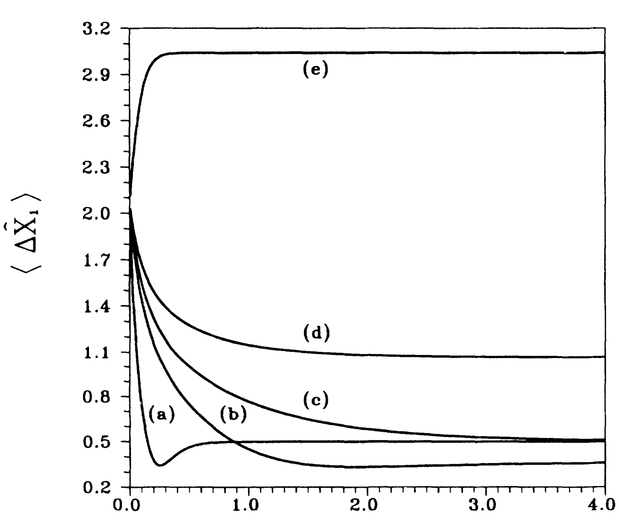

FIG. 17. Standard deviation in the field quadrature $\hat{X}_1$ for an initial even coherent state. The parameters are the same as in Fig. 12. We obtain squeezing in this quadrature for small *positive* values of Ω according to Eq. (60).

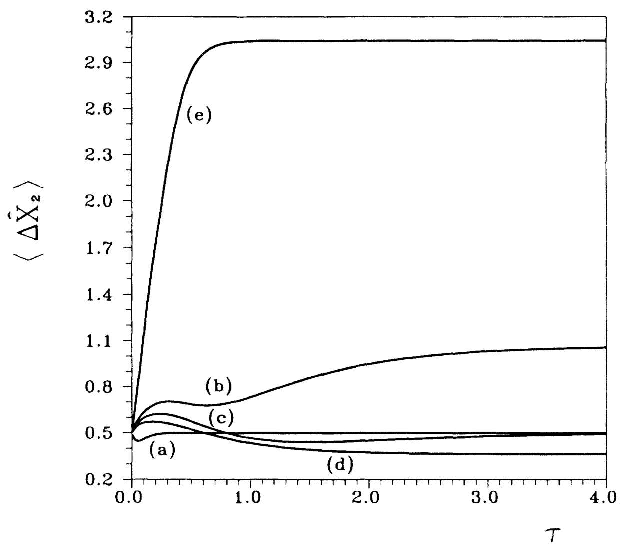

FIG. 18. Standard deviation in the field quadrature $\hat{X}_2$ for the parameters of Fig. 12. We obtain squeezing in the steady state only for small *negative* values of Ω according to Eq. (60).

$$\langle[\Delta\hat{X}_{1,2}(0)]^2\rangle=\frac{1}{4}+\frac{\bar{n}_{\rm th}}{2}\ . \tag{64}$$

We easily calculate the steady-state values

$$\langle[\Delta\hat{X}_{1,2}(\infty)]^2\rangle=P_e\langle[\Delta X_{1,2}(\infty)]^2\rangle_e +P_o\langle[\Delta\hat{X}_{1,2}(\infty)]^2\rangle_o\ , \tag{65}$$

where the amplitude variances for the even and odd coherent states are given in Eqs. (60) and (61) and the two

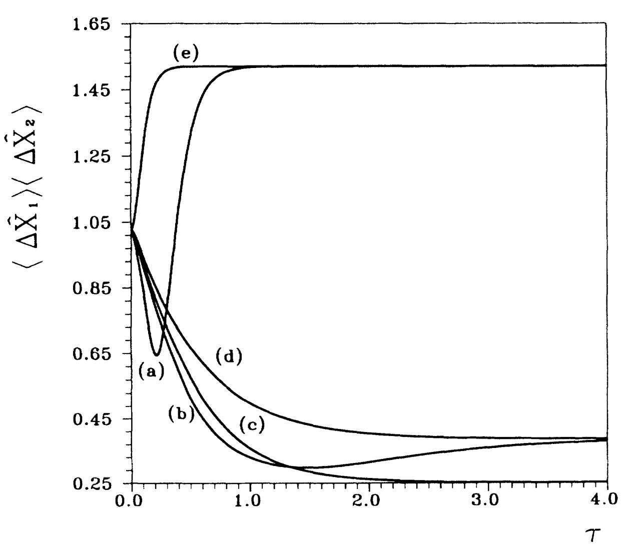

FIG. 19. Product of the uncertainties in the quadratures for the parameters of Fig. 12. The field displays extra noise in the uncertainty product. When the amplitude of the initial state is attenuated, the noise is reduced. When the initial amplitude is amplified, the field presents enhanced noise in the uncertainty product.

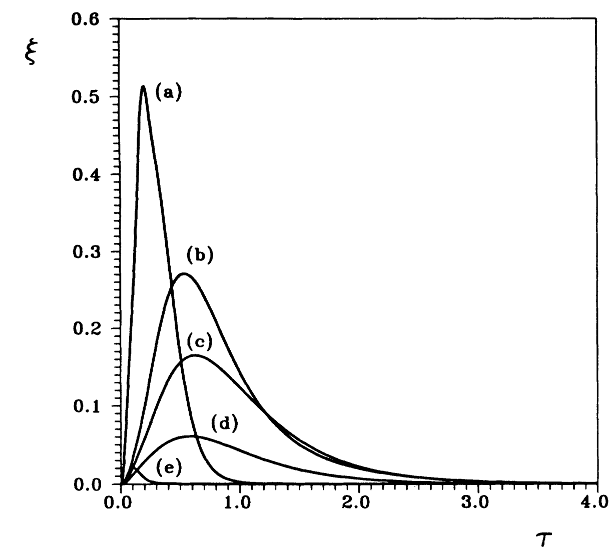

FIG. 20. The field purity ξ for the parameters of Fig. 12. We observe how as it evolves the field recovers its purity in the steady state.

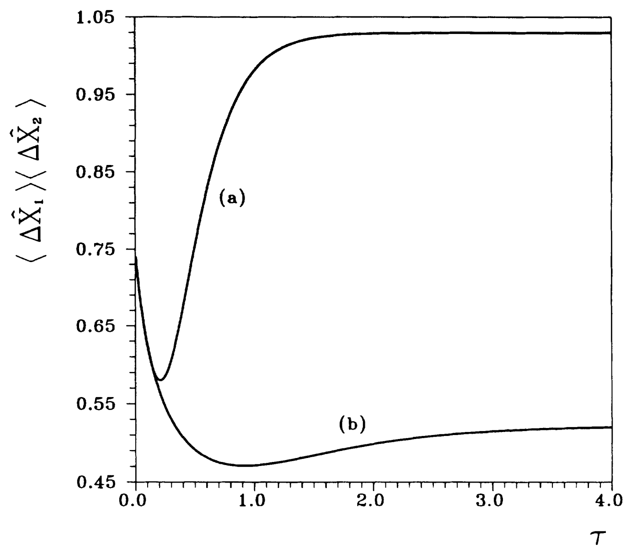

FIG. 22. Uncertainty product in $\hat{X}_1$ and $\hat{X}_2$, for the same conditions as in Fig. 15. The parameters are (a) $|\Omega|=8$ and (b) $|\Omega|=2$. We see that the field is never in a minimum-uncertainty state. Contrary to the case of the initial vacuum or one-photon states, the uncertainty product first decreases. After reaching a minimum value, it increases at a rate proportional to the coupling strength.

probabilities are given in Eq. (62). The overall evolution is very similar to the initial vacuum and one-photon state evolution. We note that the best transient squeezing is obtained for the initial vacuum. Finally, we present the uncertainty product in Fig. 22. Small values of $|\Omega|$ lead to a reduction in the uncertainty product whereas large values cause a transient reduction followed by a monotonic increase.

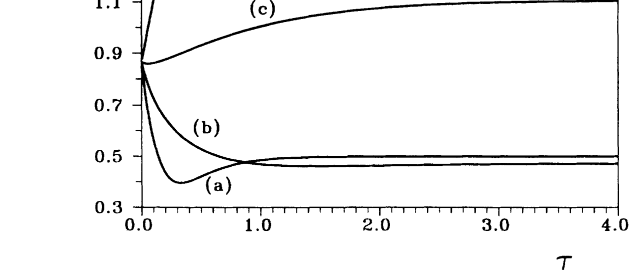

FIG. 21. Uncertainty in the amplitude quadrature $\hat{X}_1$ for the same parameters as in Fig. 15, i.e., for an initial thermal field. The values of the scaled coupling are (a) $\Omega=8$, (b) $\Omega=2$, (c) $\Omega=-2$, and (d) $\Omega=-8$. The evolution is similar to the initial vacuum case, which leads to the best transient squeezing. The uncertainty in the conjugate component $\hat{X}_2$ is obtained by changing the sign of the driving coupling constant.

C. Wigner function evolution for an initial thermal field

To conclude this section, we show a sequence of Wigner functions for the case of the initial thermal field with $\bar{n}_{\rm th}=1$ and $\Omega=8$. In Fig. 23(a) we show the initial state which has a Wigner function similar to the vacuum, but broader. When $\tau=0.5$ in Fig. 23(b) we see that the squeezing effect is dominant. We show the Wigner function at $\tau=1$ in Fig. 23(c), where the damping influence becomes apparent. When time progresses, the field evolves towards a statistical mixture of an even and an odd coherent state. In Fig. 23(d) we observe the development of fringes in the Wigner function; when $\tau=2$, the field is fairly close to its steady state.

XI. CONCLUSIONS

We have shown that quantum features occur in parameteric amplification subjected to two-photon absorption. Remarkably, initial vacuum and one-photon states evolve to steady states which are *pure states.* They are a *superposition* of two coherent states of a type that depends on the initial conditions: the initial vacuum field leads to an even coherent state whereas the one-photon state is transformed to an odd coherent state. The displacement parameter for these superposition states is simply given by the ratio of the parametric susceptibility λ and the two-photon absorption rate κ_2. We have also demonstrated that one even coherent state can be converted into another. Thus the properties of the steady-state field are those of the even and odd coherent

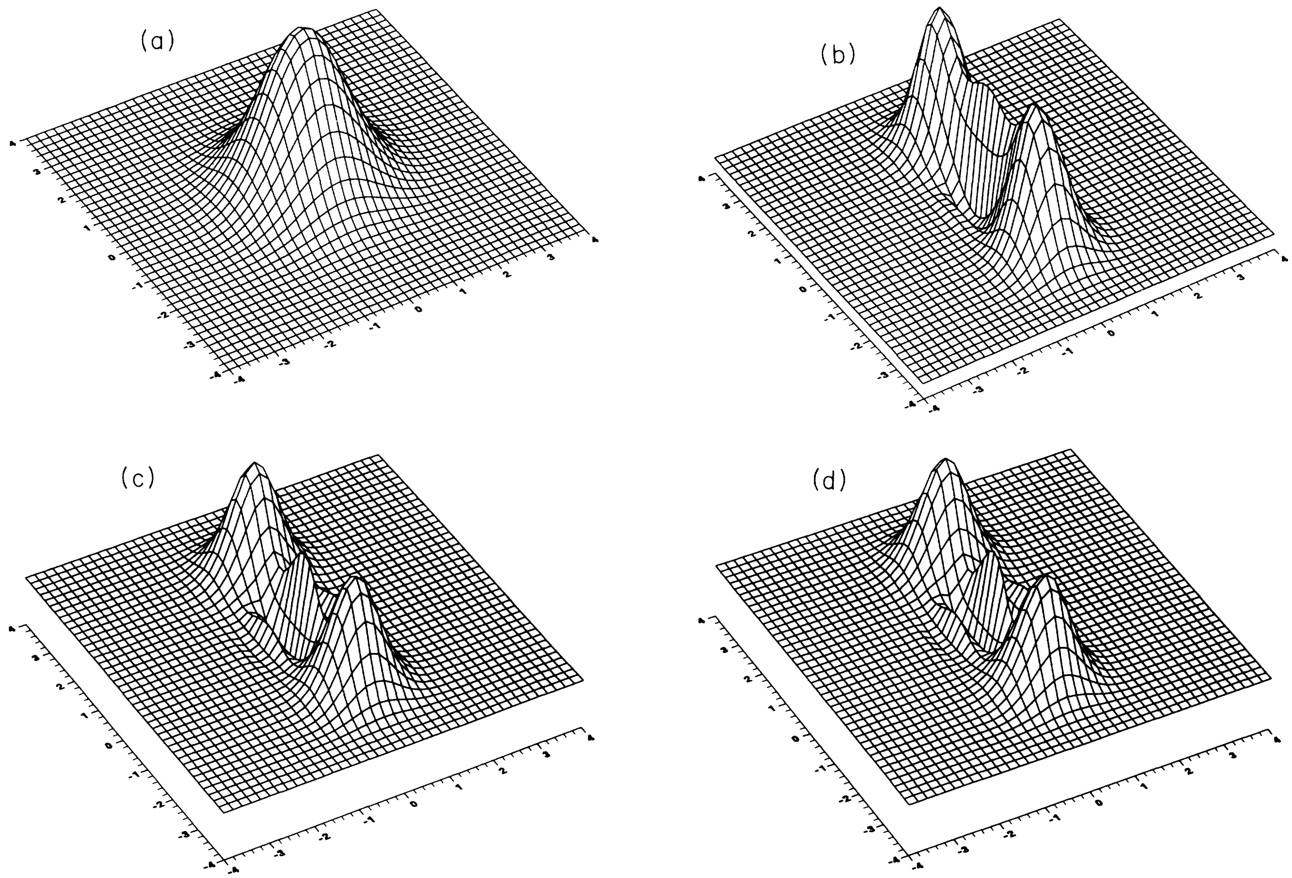

FIG. 23. We show the time evolution of the Wigner function for the initial thermal field of Fig. 14. The scaled times are (a) $\tau=0$, (b) $\tau=0.5$, (c) $\tau=1$, and (d) $\tau=2$. We can observe first the squeezing effect, followed by the development of fringes, a result of the balance between the two two-photon processes.

states—they may exhibit squeezing or sub-Poissonian photon statistics accordingly. During the transient regime there may be enhanced nonclassical features, though these depend somewhat on the parameters.

As expected we found that the one-photon losses had a very damaging effect on the purity of the state and on the fringes in the Wigner function. However, the increase in entropy found was comparable to that found for an initial cat state placed in a one-photon absorber. So it may be possible to produce fairly macroscopic superpositions of coherent states. This would be of interest in itself, even though these states would show only small squeezing or small deviations from Poissonian statistics and would be very susceptible to one-photon losses.

ACKNOWLEDGMENTS

This work was supported in part by the United Kingdom Science and Engineering Research Council and the Commission of the European Community.

[1] L. Gilles and P. L. Knight, Phys. Rev. A **48**, 1582 (1993).
[2] C. C. Gerry and E. E. Hach III, Phys. Lett. A **174**, 185 (1993); C. C. Gerry, J. Mod. Opt. **40**, 1053 (1993).
[3] E. Yablonovitch, Phys. Rev. Lett. **58**, 2059 (1987).
[4] W. H. Louisell, *Quantum Statistical Properties of Radiation* (Wiley, New York, 1973).
[5] J. A. Fleck, J. R. Morris, and M. D. Feit, Appl. Phys. **10**, 129 (1976); M. D. Feit, J. A. Fleck, and A. Steiger, J. Comput. Phys. **47**, 412 (1982); see also, e.g., K.-A. Suominen, B. M. Garraway, and S. Stenholm, Phys. Rev. A **45**, 3060 (1992).
[6] W. Magnus, Commun. Pure Appl. Math. **7**, 649 (1954).
[7] B. L. Schumaker and C. M. Caves, Phys. Rev. A **31**, 3093 (1985).
[8] H. D. Simaan and R. Loudon, J. Phys. A **11**, 435 (1978).
[9] J. Dalibard, Y. Castin, and K. Mølmer, Phys. Rev. Lett. **68**, 580 (1992); K. Mølmer, Y. Castin, and J. Dalibard, J. Opt. Soc. Am. B **10**, 524 (1993); H. J. Carmichael, *An Open Systems Approach to Quantum Optics*, Lecture Notes in Physics (Springer-Verlag, Berlin, 1993); N. Gisin and I.

C. Percival, J. Phys. A **25**, 5677 (1992); C. W. Gardiner, A. S. Parkins, and P. Zoller, Phys. Rev. A **46**, 4363 (1992); R. Dum, A. S. Parkins, P. Zoller, and C. W. Gardiner, *ibid.* **46**, 4382 (1992); H. M. Wiseman and G. J. Milburn, *ibid.* **47**, 642 (1993); **47**, 1652 (1993); B. M. Garraway and P. L. Knight, *ibid.* **49**, 1266 (1994).

[10] K. E. Cahill and R. J. Glauber, Phys. Rev. **177**, 1857 (1969).

[11] B. M. Garraway and P. L. Knight, Phys. Rev. A **46**, 5346 (1992); Phys. Scr. **T48**, 66 (1993).

[12] I. S. Gradshteyn and I. M. Ryzhik, *Table of Integrals, Series, and Products* (Academic, New York, 1980).

[13] See, for example, W. H. Zurek, Phys. Today **44** (10), 36 (1991), and references therein; V. Bužek, A. Vidiella-Barranco, and P. L. Knight, Phys. Rev. A **45**, 6570 (1992).

[14] See, for example, J. Peřina, *Quantum Statistics of Linear and Nonlinear Optical Phenomena* (Reidel, Dordrecht, 1984).

[15] J. Gea-Banacloche, Phys. Rev. Lett. **65**, 3385 (1990); Phys. Rev. A **44**, 5913 (1991); **46**, 7307 (1992); M. Brune, S. Haroche, J. M. Raimond, L. Davidovich, and N. Zagury, *ibid.* **45**, 5193 (1992); S. J. D. Phoenix and P. L. Knight, Phys. Rev. Lett. **66**, 2833 (1991); C. C. Gerry, Opt. Commun. **91**, 247 (1992); B. Sherman and G. Kurizki, Phys. Rev. A **45**, 7674 (1992); B. M. Garraway, B. Sherman, H. Moya-Cessa, P. L. Knight, and G. Kurizki, *ibid.* **49**, 535 (1994).